Random number generation with a chaotic electromechanical resonator

Guilhem Madiot, Franck Correia, Sylvain Barbay, Rémy Braive

PAPER • **OPEN ACCESS**

Random number generation with a chaotic electromechanical resonator

To cite this article: Guilhem Madiot *et al* 2022 *Nanotechnology* **33** 475204

OPEN ACCESS
IOP Publishing
Nanotechnology
Nanotechnology 33 (2022) 475204 (7pp)
https://doi.org/10.1088/1361-6528/ac86da

Random number generation with a chaotic electromechanical resonator

Guilhem Madiot[1], Franck Correia[1], Sylvain Barbay[1] and Remy Braive[1,2,3]

[1] Université Paris-Saclay, CNRS, Centre de Nanosciences et de Nanotechnologies, F-91120, Palaiseau, France
[2] Université Paris Cité, CNRS, Centre de Nanosciences et de Nanotechnologies, F-91120 Palaiseau, France
[3] Institut Universitaire de France, Paris, France

E-mail: remy.braive@c2n.upsaclay.fr

Received 27 April 2022, revised 15 June 2022
Accepted for publication 3 August 2022
Published 5 September 2022

Abstract

Chaos enables the emergence of randomness in deterministic physical systems. Therefore it can be exploited for the conception of true random number generators mandatory in classical cryptography applications. Meanwhile, nanomechanical oscillators, at the core of many on-board functionalities such as sensing, reveal as excellent candidates to behave chaotically. This is made possible thanks to intrinsic mechanical nonlinearities emerging at the nanoscale. Here we present a platform gathering a nanomechanical oscillator and its integrated capacitive actuation. Using a modulation of the resonant force induced by the electrodes, we demonstrate chaotic dynamics and study how it depends on the dissipation of the system. The randomness of a binary sequence generated from a chaotic time trace is evaluated and discussed such that the generic parameters enabling successful random number generation can be established. This demonstration makes use of concepts which are sufficiently general to be applied to the next generation of nano-electro-optomechanical systems.

Keywords: chaos, nanofabrication, photonic crystal, random number generator, electro-optomechanics

(Some figures may appear in colour only in the online journal)

1. Introduction

The combination of integrated electronics and suspended micro or nanomechanics in micro-nano electromechanical systems (M&NEMS) have led to a large number of industrial applications that have now invaded our daily lives such as, e.g. accelerometers or gyroscopes [1], all present in a modern smartphone. M&NEMS are also likely to be used as gas, mass or pressure sensors, and have also potential for bio-medical applications [2]. Although these devices generally rely on the static response of a mechanical component to an external stimulus, e.g. the acceleration provoked by a car accident in an air-bag trigger, it can also be interesting to exploit the resonance phenomena occurring in these mechanical structures. By coupling the latter with an excitation scheme, such as a piezoelectric or capacitive actuator, one can resonantly drive the mechanical motion. This configuration finds an immediate application with microphone which converts electrical signals to acoustic waves, and reciprocally. By reducing the dimensions of these electromechanical systems at the nanoscale, one can not only access the radio-frequency (RF) domain, but also unavoidably allow nonlinear phenomena to manifest in the dynamics of these devices. Interestingly such nonlinear behavior is not necessarily a drawback but can actually be exploited. Amplification of weak signals, for example, can be achieved using NEMS thanks to a bistable regime enabled by a structural Duffing anharmonicity of the material [3, 4].

Among the possible regimes achievable with such nonlinear oscillators, chaos might be the most intriguing as it

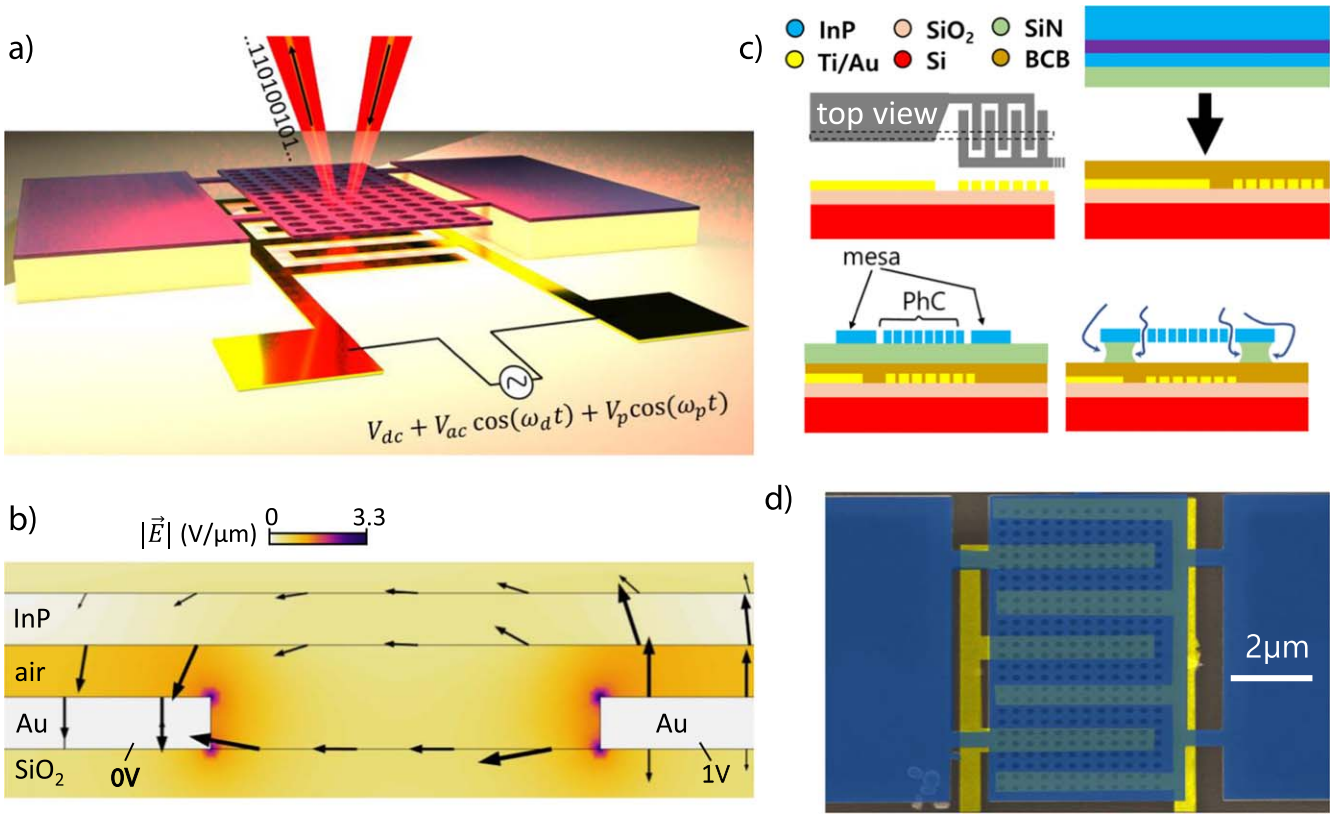

Figure 1. (a) Artistic view of the platform and random number generation encrypted in the readout optical field. (b) FEM simulation of the electric field in a simplified cross-section of the system. The black arrows show the vector field $\vec{E}$ which its norm is shown in color. (c) Fabrication process: IDE deposition by EBL and lift off, integration of an InP substrate by heterogeneous bonding, EBL definition of the mechanical structures and ICP, under-etching and CPD. (d) colorized SIM micrograph with the PhC membrane (blue) and IDT shown in transparence (yellow).

enables the introduction of unpredictability in classical and deterministic physical systems. Thus chaos emerges as a possible solution to generate true randomness without appealing to stochastic [5] or quantum [6] phenomena. In this spirit there have been several proposals to generate true random number sequences out of a chaotic time trace [7–10]. Several approaches using mechanical systems have also been considered [11–13], for pseudo-RNG applied to image encryption [14], and applied with bit-rate above 100 MHz [9, 15], but rely on an external chaotic generator.

Here we present an integrated electromechanical device based on photonic-crystal (PhC) membrane and interdigitated electrodes (IDE) separated by a nanometric air-gap (see figures 1(a) and (b)). Such a system enables controlled chaos to emerge using a slowly-modulated electromechanical force [16–18]. An in-depth study of chaotic dynamics is performed upon the mechanical dissipation. Applying a threshold to generate random binary sequences from chaotic time traces, we evaluate the randomness quality as a function of two parameters involved in the sequence generation. Importantly, this study goes way beyond the scope of our system and could be applied to any system displaying similar driven chaotic dynamics [17].

Our experiment, which gathers both electromechanical actuation and optical readout aided by an integrated optical cavity, enables the transduction of the mechanical motion into the optical domain. This ability to gather electromechanical and optical properties within the same device constitutes the basis for the development of nano-opto-electro-mechanical systems (NOEMS) [19–22]. The multiplication of such novel platforms respond the interest focused to specific functionalities, such as optical-to-RF conversion [23–25], or opto-electro-mechanical switches [26, 27], for example.

2. System description and nanofabrication

To gather the mechanical, electrical and optical properties into such NOEMS, we base the design on a 260 nm thick suspended indium phosphide (InP) membrane. This 20×10 μm^2 rectangular membrane constitutes a mechanical resonator whose quality factor can be significantly increased by optimizing the four bridges connecting the membrane to the substrate [28]. Electromechanical actuation is enabled by the integration of IDE below the free-standing membrane. The latter is engineered as an optical reflector by etching it through with a 2D photonic crystal which maximizes its normal reflexion coefficient [29].

The main steps of the nanofabrication process flow are schematically depicted in figure 1(c). They include (a) the electron beam lithography (EBL) of the IDE on a silicon wafer, followed by metal deposition and lift off; (b) the

heterogeneous BCB-bonding [30] on the Si wafer of an InP substrate incorporating the InP membrane onto which 350 nm of SiN is deposited by PECVD and chemical InP substrate removal; (c) the EBL patterning of the mechanical structures and photonic crystals followed by ICP etching of the InP layer; and (d) under-etching of the mechanical structure (etching of the SiN layer) with HF, followed by critical point drying. The resulting platform is shown in the colorized SEM micrograph in figure 1(d).

The 350 nm air gap separating the membrane from the IDE placed below constitutes an optical cavity at the He–Ne wavelength (633 nm). This optomechanical readout permits to enhance the sensitivity to detect the membrane out-of-plane resonances [31]. Meanwhile the dielectric properties of the membrane make it easier to be excited by capacitive actuation. Both DC gate V_{dc} and RF signal $V_{\mathrm{ac}}\cos(2\pi f_{\mathrm{d}}\,t)$ are applied externally between these two electrodes and the field lines penetrate and polarize the InP membrane. In figure 1(b), we show the stationary solution for the electric vector field $\overrightarrow{E}$ (arrows) and norm $|\overrightarrow{E}|$ (colorscale) in the system, obtained by Finite-Element Simulation methods. This model accounts for a 2D cross-section of the structure, with electrical potential of 1 V imposed every two gold digits while the others are grounded. This produces electric field arcs that cross the above InP membrane, which induces on it a capacitive force $F_{\mathrm{ec}} \propto V_{\mathrm{tot}}^2$. Neglecting non-resonant terms of F_{ec} results in a near-resonant force $F_{f_d}(t) \propto V_{\mathrm{ac}} V_{\mathrm{dc}} \cos(2\pi f_{\mathrm{d}}\,t)$. Therefore when the actuation frequency f_{d} approaches a mechanical resonance f_{m}, the mechanical oscillation amplitude of the membrane increases. With this system, we are interested in probing the first order mode of the membrane which has the highest overlap with the incident optical field. This 'drum' mode has the strongest out-of-plane amplitude and therefore is prone to exhibit nonlinearity, which is essential in the following to obtain a chaotic dynamics.

3. Dissipation parameters control and influence on chaotic dynamics

The sample is placed in a vacuum chamber pumped at 10^{-6} mbar. The He–Ne laser is focused at the center of the membrane. Several mechanical modes are observed between 2 and 15 MHz. As discussed above, we focus on the fundamental mode, with frequency $f_{\mathrm{m}} = 2.327$ MHz. The associated IDE is submitted to a voltage $V_{\mathrm{dc}} + V_{\mathrm{ac}}\cos(2\pi f_{\mathrm{d}}\,t)$ with $V_{\mathrm{dc}} = 2$ V and $V_{\mathrm{ac}} = 0.5$ V. While scanning the driving frequency f_{d} around the mechanical resonance, we demodulate the photo-received optical signal with a passband filter centered at f_{d} and 100 Hz wide, returning both demodulated amplitude V and phase φ. The amplitude voltage can be converted into a mechanical displacement r after calibration.

This measurement is reproduced for different values of the pressure in the vacuum chamber and four representative spectral responses are shown in figure 2(a). We note a significant broadening of the mechanical resonance while the pressure increases. This results from the increasing

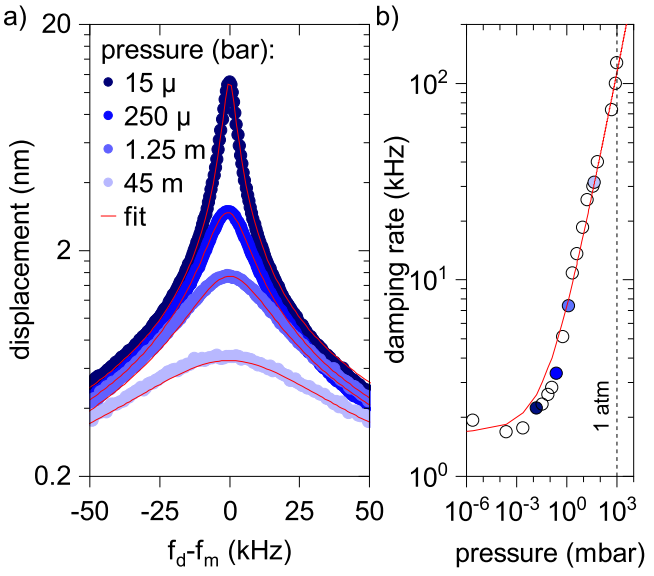

Figure 2. (a) Normalized spectral response of the mechanical mode at different pressure condition in the vacuum chamber with Lorentzian fits (red lines). (b) Pressure dependence of the mechanical damping dots, with a power-law fit (red line).

contribution of air-damping in the mechanical dissipation. We fit each resonance curve with the Lorentzian lineshape (red lines) and extract the mechanical damping rate. The latter is plotted as a function of the pressure in figure 2(b). An exponential increase is observed above 1 mbar while a saturation to $\gamma_0 \sim 2$ kHz is observed below this value. The saturation arises when the mechanical losses are no longer dominated by air-damping but rather explainable by internal mechanical loss channels such as clamping and thermo-mechanical losses.

So far we have used sufficiently low input voltages V_{ac} and V_{dc} for the mechanics to remain in the linear regime, where the system can be treated as a driven harmonic oscillator. Increasing the electromechanical force applied on these membranes leads to a distortion of the resonance, which can become bistable above a threshold. Such behaviour is typical of a Duffing oscillator, which consists in a nonlinear oscillator with a third order anharmonicity β in its equation of motion of the oscillator:

$$\ddot{x} + 2\pi\gamma_0\dot{x} + (2\pi f_m)^2 x + \beta x^3 = F_{f_d}(t). \qquad (1)$$

This equation is commonly used to model nonlinear mechanical resonances [3, 4], among others. The bistable resonance can be observed by scanning f_d forward and backward around the mechanical frequency. Such measurement is shown in figure 3(a) at three different values of the vacuum chamber pressure. The data are normalized by their respective maximum and the linear lineshape (see figure 2(a)) are reported here for reference. In each case we apply the same excitation with $V_{\mathrm{ac}} = 3$ V. We note that a relatively small increase of the mechanical linewidth provokes a significant change in the bistability, whose frequency span tends to reduce.

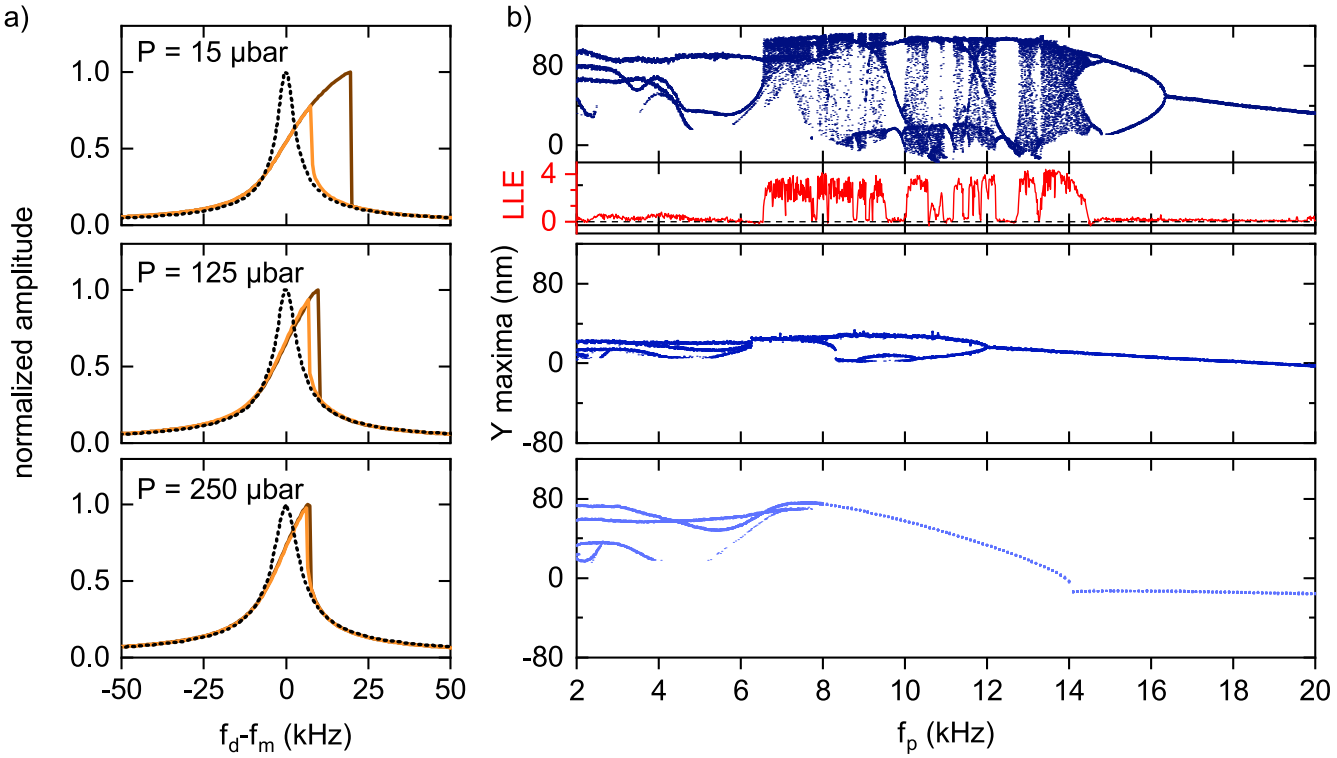

Figure 3. For a vacuum chamber internal pressure of 15 μbar (top), 125 mbar (center) and 250 mbar (bottom), we show: (a) the normalized mechanical displacement with forward (brown) and backward (orange) sweep of the driving frequency around mechanical frequency $f_m = 2.327$. The linear response is indicated for reference (back dashed). (b) An experimental bifurcation diagram parametrized with the pump frequency f_p. While the latter is swept from 2 to 20 kHz, a Poincaré section is built from the maxima of the quadrature $Y(t)$, and plotted as a function of f_p. A period-doubling cascade is observed for decreasing f_p, but chaos is only observed at sufficiently low pressure, as confirmed by the largest Lyapunov exponent (LLE) plotted in red for the top diagram.

In the following we induce a chaotic dynamics by performing an amplitude modulation of the electromechanical force [16–18, 31]. We add a new component $V_p \cos(2\pi f_p t)$ to the voltage applied to the IDE and we refer to it as the pump signal. It leads to a modulation at frequency f_p of the electrocapacitive force resonant component, which now writes $F_{f_d}(t) \propto V_{dc}(V_{ac} + V_p \cos(2\pi f_p t))\cos(2\pi f_d t)$. The driving frequency f_d is set at the low-frequency edge of the bistability, ensuring a wider bandwidth for the chaotic regime [16].

Both the pump amplitude V_p and frequency f_p can be played with to tune the dynamical regime of mechanical responses. Increasing the amplitude for a fixed frequency typically leads to a period-doubling cascade route to chaos [31]. Here we rather set the pump amplitude to $V_p = 2.5$ V and scan the frequency from 2 to 20 kHz. The mechanical response time traces $r(t)$ and $\varphi(t)$ are recorded for 100 ms. The quadrature $Y(t) = r(t)\sin(\varphi(t))$ is used to reconstruct a Poincaré section of the signal. The latter is plotted as a function of f_p in the bifurcation diagrams shown in figure 3(b).

At low pressure, the mechanical displacement induces sufficiently strong nonlinearity to enable a driven chaotic dynamics, as illustrated at $P = 15$ μbar. The cascaded period-doubling to chaos is observed for decreasing f_p, and starts around 16.5 kHz. The presence of chaos can be numerically verified by computing the largest lyapunov exponent, that we show in red below this bifurcation diagram. A zero LLE indicates a periodic or quasi periodic motion whereas a strictly positive LLE corresponds to a chaotic dynamics. The presence of experimental noise slightly increases the LLE giving rise to a slightly positive value even for periodic motion but the significant increase at some specific positions —from 6.6 to 14.5 kHz—clearly indicates the range of f_p in which chaos emerges. These regions are also visually identifiable on the diagram as they translate into a dense Poincaré section. Here the chaos spans over ~8 kHz but this range tends to reduce when the mode linewidth increases, since this comes also with a decrease of the mechanical nonlinearity, the bistability span being strongly dependent on the damping rate. Thus at 125 μbar the bifurcation diagram does not display a chaotic regime although a period-doubling is observed at ~12 kHz. The dynamics keeps getting poorer as the pressure in the chamber increases, as illustrated with the third panel taken at 250 μbar.

4. Random number generation

Now that we have described the conditions under which chaos can be reached, we can focus on the exploitation of this dynamical regime to generate random numbers. Here we apply a method enabling the production of a sequence of random bits from an experimental chaotic time trace. This is achieved using a method described in [32] where the sign of a

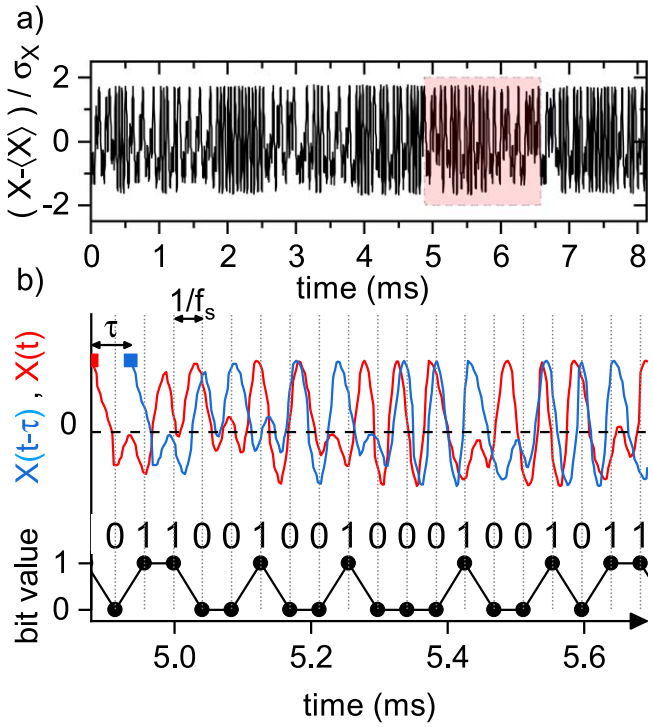

Figure 4. (a) Experimental chaotic time trace. (b) The trace $X(t)$ is compared to its delayed self $X(t-\tau)$. (c) The XOR logical gate is periodically applied to the traces relative sign. It results in a binary sequence.

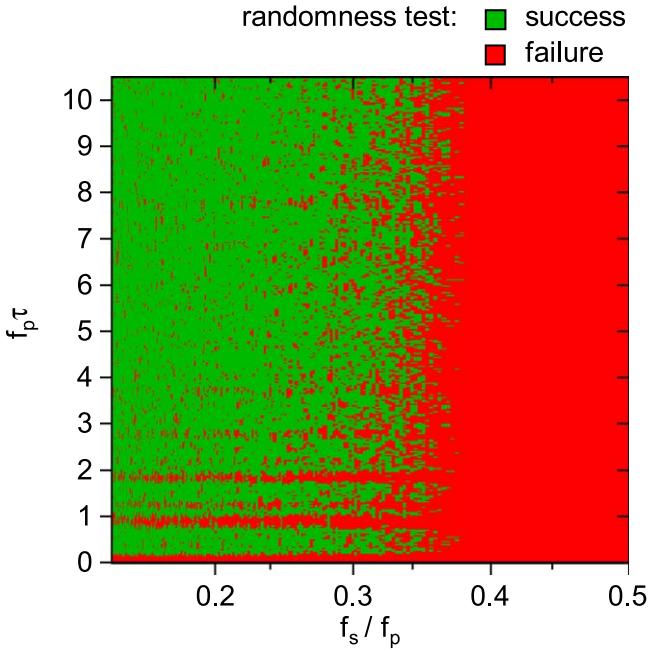

Figure 5. Randomness test suite result as a function of the delay τ and the sampling frequency f_s applied to the trace presented in figure 4(a). Both x- and y-axis are shown in units of modulation periods.

time trace is periodically compared to a delayed copy of itself with the logical function XOR. We record the quadrature $X(t) = r(t)\cos(\varphi(t))$ for $f_p = 12.3$ kHz and $V_p = 2.5$ V. In practice, we consider the normalized time trace $(X - \langle X\rangle)/\sigma_X$ where $\langle X\rangle$ and σ_X are the mean value and the standard deviation of $X(t)$ calculated over the full time trace, respectively. Note that the following results remain unchanged by using the other quadrature, $Y(t)$. The normalized time trace under study is shown in figure 4(a). We introduce a delay τ and a sampling frequency f_s, which corresponds to the rate at which $X(t)$ and $X(t-\tau)$ will be compared (see figure 4(b)). The bits resulting from the XOR gate applied between the respective signs of these two traces are shown in figure 4(c).

In the following the randomness of a binary sequence is verified by applying the NIST Statistical Test Suite [33]. It is composed by 14 randomness tests, each returning a p-value that can be interpreted as the probability for the sequence to be random according to the corresponding test. The p-value validates the test if its value is above 0.01. In the following we simply apply all these algorithms on our binary sequence and check the p-values. If all the p-values validate the sequence as random, we consider that this sequence passes the randomness test. On the contrary, if at least one test fails, we consider the sequence as not random.

Our objective is to characterize the randomness test success as a function of the delay τ and the sampling frequency f_s. By generating a binary sequence for several values of τ and f_s, we plot a matrix showing the randomness test result in figure 5. The green (resp. red) pixels correspond to a successful (resp. unsuccessful) test. Both the sampling frequency and the delay are shown in units of pump frequency and pump period, respectively. f_p^{-1} corresponds to the mean oscillation period of the chaotic trace. We observe a significant increase of the randomness quality towards low sampling frequencies, with a threshold limit around 0.35. This is related to the modulation frequency f_p in the present case. Indeed at high sampling frequencies, the trace does not have enough time to evolve between two samples. This favors the apparition of runs of ones and zeros ('00', '11', '000', '111', and so on) which breaks the sequence randomness. Moreover the randomness quality shows significant degradation at $f_p\tau = 1$ and 2. This relates with a strong correlation between $X(t)$ and $X(t-\tau)$ for these values of the delay. Overall, low sampling frequency and high delay improve the randomness of the sequence. Randomness can emerge only if τ is sufficiently high for the two traces to decorrelate. Beyond these specific points, figure 5 evidences many pairs of delay and sampling frequency allowing random number generation.

Here, the ability to extract randomness from chaos fully relies on a deterministic chaotic dynamics that can be theoretically modelled with the Duffing oscillator [31]. It is possible to evaluate this chaos entropy [34] and to improve it by different methods such as bandwidth enhancement [32] or using electrical noise [5].

5. Conclusion

We have presented a nano-electromechanical system displaying driven chaotic dynamics when submitted to a periodically time-varying force. In a first experiment, we submit the mechanical system to different environmental condition,

by controlling the pressure in the vacuum chamber. From the dissipative properties of the system, we conclude on their effect on the dynamics of the nonlinear system. The emergence of chaos is clearly favoured by a higher mechanical quality factor, as this comes with a more pronounced bistability.

Using a chaotic time trace to generate binary sequences, we study the randomness of the latter as a function of two control parameter. We draw general conclusions about the respective influence of these two buttons, and relate these dependencies with the physics of the system. RNG in a driven chaotic system such as the one presented here could benefit from the use of two quadratures while only one is considered here. Simultaneous generation of random bits using both quadratures could multiply the bit-rate by two, and even more in multimode systems, if several drives and demodulation channels are used at the same time [31]. In order to improve the sequences randomness, one could rather compare two chaotic signals simultaneously provided by two fully uncoupled electromechanical resonators. This strategy only requires a common RF driving signal for the two—which will most likely trigger two different chaotic dynamics due to inherent nanofabrication disorder—and improve the randomness by reducing the correlation between the traces. Alternatively, new nonlinear mechanical regimes [35] can be explored if the mechanical Q-factor is significantly improved, e.g. by engineering the mechanical loss channels [36]. These new regimes might reveal chaotic regimes enabling higher randomness quality.

In addition, the dynamics under study here is scalable, i.e. it could be reproduced in other types of devices, performing at higher frequencies, and relying on a different physics. The condition for chaos to emerge relies (1) on the presence of an intrinsic nonlinearity triggering bistable behaviours in the system, and (2) on the time-modulation of the driving force. Self-sustained optomechanical GHz oscillators [37, 38] could be exploited to reproduce these results at higher frequency, potentially increasing the bit rate to several Gbps.

Acknowledgments

This work is supported by the French RENATECH network, the European Union's Horizon 2020 research innovation program under grant agreement No. 732894 (FET Proactive HOT), the Agence Nationale de la Recherche as part of the 'Investissements d'Avenir' program (Labex NanoSaclay, ANR-10-LABX-0035) with the flagship project MaCaCQu and the JCJC project ADOR (ANR-19-CE24-0011-01).

Data availability statement

The data that support the findings of this study are available upon reasonable request from the authors.

ORCID iDs

Guilhem Madiot https://orcid.org/0000-0003-2662-4324
Sylvain Barbay https://orcid.org/0000-0003-0092-7829
Remy Braive https://orcid.org/0000-0002-7816-9530

References

[1] Bogue R 2007 Mems sensors: past, present and future *Sensor Rev.* **27** 7–13
[2] Bhansali S and Vasudev A 2012 *MEMS for Biomedical Applications* (Amsterdam: Elsevier)
[3] Chowdhury A, Barbay S, Clerc M G, Robert-Philip I and Braive R 2017 Phase stochastic resonance in a forced nanoelectromechanical membrane *Phys. Rev. Lett.* **119** 234101
[4] Chowdhury A, Clerc M G, Barbay S, Robert-Philip I and Braive R 2020 Weak signal enhancement by nonlinear resonance control in a forced nano-electromechanical resonator *Nat. Commun.* **11** 2400
[5] Gong L, Zhang J, Liu H, Sang L and Wang Y 2019 True random number generators using electrical noise *IEEE Access* **7** 125796
[6] Vallone G, Marangon D G, Tomasin M and Villoresi P 2014 Quantum randomness certified by the uncertainty principle *Phys. Rev.* A **90** 052327
[7] Sciamanna M and Shore K A 2015 Physics and applications of laser diode chaos *Nat. Photon.* **9** 151–62
[8] Kim M, Ha U, Lee K J, Lee Y and Yoo H-J 2017 A 82-nw chaotic map true random number generator based on a sub-ranging sar adc *IEEE J. Solid-State Circuits* **52** 1953–65
[9] Shi B, Luo C, Flores J G F, Lo G, Kwong D-L, Wu J and Wong C W 2020 Gbps physical random bit generation based on the mesoscopic chaos of a silicon photonics crystal microcavity *Opt. Express* **28** 36685–95
[10] Yu F, Li L, Tang Q, Cai S, Song Y and Xu Q 2019 A survey on true random number generators based on chaos *Discrete Dyn. Nat. Soc.* **2019** 1–10
[11] Voris J, Saxena N and Halevi T 2011 Accelerometers and randomness: perfect together *Proc. Fourth ACM Conf. on Wireless Network Security, WiSec '11* (New York, NY: Association for Computing Machinery) pp 115–26
[12] Liao T-L, Wan P-Y and Yan J-J 2019 Design of synchronized large-scale chaos random number generators and its application to secure communication *Appl. Sci.* **9** 185
[13] Dantas W G, Rodrigues L R, Ujevic S and Gusso A 2020 Using nanoresonators with robust chaos as hardware random number generators *Chaos* **30** 043126
[14] Haliuk S, Krulikovskyi O, Vovchuk D and Corinto F 2022 Memristive structure-based chaotic system for prng *Symmetry* **14** 68
[15] Garcia-Bosque M, Pérez A, Sánchez-Azqueta C and Celma S 2017 Application of a mems-based trng in a chaotic stream cipher *Sensors* **17** 646
[16] Defoort M, Rufer L, Fesquet L and Basrour S 2021 A dynamical approach to generate chaos in a micromechanical resonator *Microsyst. Nanoeng.* **7** 1–11
[17] Houri S, Asano M, Yamaguchi H, Yoshimura N, Koike Y and Minati L 2020 Generic rotating-frame-based approach to chaos generation in nonlinear micro- and nanoelectromechanical system resonators *Phys. Rev. Lett.* **125** 174301
[18] Miles J 1984 Chaotic motion of a weakly nonlinear, modulated oscillator *Proc. Natl Acad. Sci.* **81** 3919–23

[19] Zobenica Ž *et al* 2017 Integrated nano-opto-electro-mechanical sensor for spectrometry and nanometrology *Nat. Commun.* **8** 2216
[20] Midolo L, Schliesser A and Fiore A 2018 Nano-opto-electro-mechanical systems *Nat. Nanotechnol.* **13** 11–8
[21] Xu N, Cheng Z-D, Tang J-D, Lv X-M, Li T, Guo M-L, Wang Y, Song H-Z, Zhou Q and Deng G-W 2021 Recent advances in nano-opto-electro-mechanical systems *Nanophotonics* **10** 2265–81
[22] Navarro-Urrios D, Colombano M F, Arregui G, Madiot G, Pitanti A, Griol A, Makkonen T, Ahopelto J, Sotomayor-Torres C M and Martínez A 2022 Room-temperature silicon platform for ghz-frequency nanoelectro-opto-mechanical systems *ACS Photon.* **9** 413–9
[23] Bochmann J, Vainsencher A, Awschalom D D and Cleland A N 2013 Nanomechanical coupling between microwave and optical photons *Nat. Phys.* **9** 712–6
[24] Bagci T *et al* 2014 Optical detection of radio waves through a nanomechanical transducer *Nature* **507** 81–5
[25] Balram K C, Davanço M I, Song J D and Srinivasan K 2016 Coherent coupling between radiofrequency, optical and acoustic waves in piezo-optomechanical circuits *Nat. Photon.* **10** 346–52
[26] Liu T, Pagliano F and Fiore A 2017 Nano-opto-electro-mechanical switch based on a four-waveguide directional coupler *Opt. Express* **25** 10166–76
[27] Haffner C *et al* 2019 Nano-opto-electro-mechanical switches operated at cmos-level voltages *Science* **366** 860–4
[28] Chowdhury A 2016 Mechanical nonlinear dynamics of a suspended photonic crystal membrane with integrated actuation *PhD Thesis* Université Paris Saclay COmUE
[29] Antoni T *et al* 2011 Deformable two-dimensional photonic crystal slab for cavity optomechanics *Opt. Lett.* **36** 3434–6
[30] Karle T J *et al* 2010 Heterogeneous integration and precise alignment of inp-based photonic crystal lasers to complementary metal-oxide semiconductor fabricated silicon-on-insulator wire waveguides *J. Appl. Phys.* **107** 063103
[31] Madiot G, Correia F, Barbay S and Braive R 2021 Bichromatic synchronized chaos in driven coupled electro-optomechanical nanoresonators *Phys. Rev.* A **104** 023525
[32] Hirano K, Yamazaki T, Morikatsu S, Okumura H, Aida H, Uchida A, Yoshimori S, Yoshimura K, Harayama T and Davis P 2010 Fast random bit generation with bandwidth-enhanced chaos in semiconductor lasers *Opt. Express* **18** 5512–24
[33] Bassham L E *et al* 2010 *SP 800-22 Rev. 1a. A Statistical Test Suite for Random and Pseudorandom Number Generators for Cryptographic Applications* (Gaithersburg, MD: NIST) Technical report
[34] Guo X, Liu T, Wang L, Fang X, Zhao T, Virte M and Guo Y 2020 Evaluating entropy rate of laser chaos and shot noise *Opt. Express* **28** 1238–48
[35] Ochs J S, Rastelli G, Seitner M, Dykman M I and Weig E M 2021 Resonant nonlinear response of a nanomechanical system with broken symmetry *Phys. Rev.* B **104** 155434
[36] Bereyhi M J, Arabmoheghi A, Beccari A, Fedorov S A, Huang G, Kippenberg T J and Engelsen N J 2022 Perimeter modes of nanomechanical resonators exhibit quality factors exceeding 10^9 at room temperature *Phys. Rev.* X **12** 021036
[37] Ghorbel I *et al* 2019 Optomechanical gigahertz oscillator made of a two photon absorption free piezoelectric III/V semiconductor *APL Photon.* **4** 116103
[38] Gomis-Bresco J *et al* 2014 A one-dimensional optomechanical crystal with a complete phononic band gap *Nat. Commun.* **5** 4452